Received: 12 April 2023 | Revised: 8 June 2023 | Accepted: 15 June 2023

DOI: 10.1002/app.54345

RESEARCH ARTICLE

Journal of Applied Polymer Science WILEY

Novel hybrid electrospun poly(ε-caprolactone) nanofibers containing green and chemical magnetic iron oxide nanoparticles

Johar Amin Ahmed Abdullah[1] | **Víctor Perez-Puyana**[2] | **Antonio Guerrero**[1] | **Alberto Romero**[2]

[1]Departamento de Ingeniería Química, Escuela Politécnica Superior, Universidad de Sevilla, Sevilla, Spain

[2]Departamento de Ingeniería Química, Facultad de Química, Universidad de Sevilla, Sevilla, Spain

Correspondence
Johar Amin Ahmed Abdullah, Departamento de Ingeniería Química, Escuela Politécnica Superior, Universidad de Sevilla, 41011, Sevilla, Spain.
Email: jabdullah@us.es

Funding information
MCIN/AEI/10.13039/501100011033/ FEDER, UE, Grant/Award Number: PID2021124294OBC21

Abstract

This study investigates the effects of incorporating green and chemical magnetic iron oxide nanoparticles (GMIONPs and CMIONPs, respectively) into poly (ε-caprolactone) (PCL) nanofibrous membranes on their physicochemical, mechanical, morphological, and functional properties. The study evaluates the physicochemical and optical properties of the nanofibrous membranes using water contact angle (WCA), water vapor permeability (WVP), brightness, color determination, UV–visible and gap energy, and light transmission. The mechanical properties were evaluated using Young's modulus, maximum stress ($б_{max}$, MPa), and the strain at break (ε_{max}), while the morphological properties were evaluated using confocal microscopy, scanning electron microscopy (SEM), and transmission electron microscopy (TEM). Functional properties were assessed in terms of antioxidant activity. The results show that incorporating MIONPs significantly affects the properties of the nanofibrous membranes. PCL/GMIONPs membranes exhibit better performance in terms of physicochemical, morphological, and functional properties than PCL/CMIONPs membranes. These findings suggest that PCL/MIONPs nanofibrous membranes could be a promising material for various biomedical applications. The incorporation of different types of magnetic iron oxide nanoparticles into PCL electrospun membranes is an innovative approach that opens up a wide range of potential applications.

KEYWORDS

antioxidant activity, electrospinning, hydrophobicity, magnetic iron oxide, nanoparticles, PCL, roughness

1 | INTRODUCTION

The electrospinning (ES) process is a fiber- or nanofiber-making technology that involves the acceleration of a jet of charged polymer solution under a controlled high-voltage electric field, leading to the creation of an interconnected film of nanofibers upon the surface of a drum collector.[1,2] A variety of polymers or polymer blends can be electrospun into nanofibers or nanofiber mats via ES[3,4] with additional materials in the form of

nano-scale particles[5–7] or incorporating molecules into functional systems.[8–10] The ES can be carried out using a wide variety of material compositions and processing conditions to achieve a wide variety of applications, such as biomedical, biotechnological, and tissue engineering applications,[11–13] gas or liquid filtration,[14–16] and harvesting and storage of energy,[17–19] including hydrogen (H_2) production, water purification, environmental protection,[20–23] and catalytic applications.[24–26]

Poly(ε-caprolactone) (PCL) is a well-known aliphatic polymer that has been widely employed to create a broad range of synthetic nanofibers, due to its excellent features, for example, biodegradability, biocompatibility, bioresorbability, hydrophobicity, easy processability, and non-toxicity.[1,22] In addition to its intrinsic hydrophobic character, electrospun PCL nanofibers might also exhibit higher biocompatibility and hydrophilicity if they are modified with surface coatings, polydopamine treatments, plasma treatments, alkali treatments, polymer grafting, or using copolymer blends, making them an attractive material for a variety of biomedical applications.[27] For example, it has been observed that the combination with pluronic increases the surface roughness of electrospun PCL nanofibers, which improves the adsorption of proteins and cells.[28] Electrospun PCL-nanofiber scaffolds have also been modified with alkaline hydrolysis to induce hydrophilicity and wettability, resulting in effective cell growth.[29,30] In terms of packaging functions, the most relevant aspects are containment, protection, convenience, and communication. The deterioration of lipid-rich foods during storage, caused by microorganisms and oxygen spoilage, results in a substantial loss of economic value. The oxidation of food products significantly shortens their shelf life. During oxidation, food loses its natural value and energy, creating undesirable odors, flavors, and pigments in the food that make it less appealing. Since rancidity and the mentioned changes are a result of free radical chains, food packaging manufacturers are constantly seeking innovative methods to reduce lipid oxidation.[31]

Nanoparticles' incorporation into polymer-based materials may solve this problem due to their excellent antioxidant and antimicrobial activity, surface-enhanced Raman scattering activity, and electrical conductivity.[4,32,33] In this sense, a synergistic combination of specific, optical, electrical, unique, catalytic, and functional properties of metal nanoparticles and polymer nanofiber materials (metal-polymer nanocomposites) has attracted a great deal of attention during the past few years. This is attributed to the excellent surface area of polymer nanofibers and the interaction between metal nanoparticles and polymer nanoparticles. A variety of metal oxide nanoparticles, including nanofillers, have been incorporated into polymer-based films/nanofibers mats in order to improve their properties.[34–41]

As one of the most commonly used nanoparticles, magnetic iron oxide nanoparticles (MIONPs) have been employed in a wide range of applications due to their advantageous characteristics, including specificity, uniqueness, magneticity, and biocompatibility.[42] MIONPs exhibit a high inhibition ability against diverse foodborne pathogens' growth.[43] These nanoparticles can liberate the reactive oxygen species that damage bacteria DNA and proteins by impairing mitochondrial function and keeping non-bacterial cells unharmed.[41,42,44] MIONPs have been reported as danger-free, non-cytotoxic, and potential oral therapy to treat iron deficiency.[44,45] Generally, these nanoparticles may vary depending on the method used for their production, since they can be synthesized in a variety of ways, including traditional and environmentally friendly methods. The traditional method typically involves the use of chemical-reducing agents (such as NaOH), which can lead to the formation of impurities and potentially hazardous substances within the nanoparticles. As an alternative to these toxic reducing agents, the green method based on a green reducing agent (polyphenol-rich plant extracts) is used to produce smaller, purer, non-toxic, less aggregated, more stable nanoparticles with high functionality.[46,47]

The incorporation of nanoparticles with different properties into polymer matrices is a promising strategy for creating materials with unique properties. However, the traditional method of mechanically mixing nanoparticles into polymer solutions often results in uneven particle distribution. To address this issue, this study utilized N,N-dimethylformamide (DFM) to reduce metal ions to zero-valent metal, resulting in the homogeneous dispersion of green and chemically synthesized magnetic iron oxide nanoparticles (GMIONPs and CMIONPs) in PCL electrospun membranes. Therefore, the main objective of this study was to analyze the effect of different concentrations of GMIONPs and CMIONPs on the physicochemical, mechanical, morphological, and biological properties of PCL nanofiber membranes. This approach offers a novel and promising approach for developing nanofibrous materials with enhanced properties for various biomedical applications.

2 | MATERIALS AND METHODS

2.1 | Materials

PCL $(C_6H_{10}O_2)_n$ (with average Mn 80,000; Sigma Aldrich, Saint Louis, Mi USA), chloroform (Friendemann Schmidt, Parkwood, Australia): DMF $(CH_3)2NC(O)H$ (Merck,

Darmstadt, Germany), gallic acid ($C_7H_6O_5$), and DPPH (2,2-diphenyl-1-picrylhydrazyl) were purchased from Sigma Aldrich. The other substances and reagents used in this study were all of analytical grade.

GMIONPs (12 ± 1 nm, 84% cubic Fe_3O_4: 16% monoclinic Fe_2O_3 and 95% crystallinity) and CMIONPs (24 ± 1 nm, 72% cubic Fe_3O_4: 28% trigonal with rhombohedral axis Fe_2O_3 and 93% crystallinity) were synthesized based on previous studies.[48–50] Briefly, the process involves mixing 20 mL of total polyphenol content (39 ± 2 mg GAE/g extract) extracted from *Phoenix dactylifera* L. (as a reducing agent) with 20 mL of ferric trichloride hexahydrate $FeCl_3{\cdot}6H_2O$ (as a precursor). The pH of the resulting mixture was adjusted to 7.5 by adding 5 M of NaOH. Then the mixture was heated at 50°C for 2 h under continuous stirring. Following this, the precipitate obtained was filtered, washed with ethanol, and dried in an oven at 100°C for 8 h. After that, it was calcined in a muffle at 500°C for 5 h.

2.2 | ES process

Solution ES was used to prepare PCL/GMIONPs and PCL/CMIONPs membranes in accordance with the methods described in a previous study with small modifications.[1] PCL was first dissolved in a co-solvent of chloroform: DMF (9:1 v/v) and stirred at room temperature to obtain the ES dope solution (10% w/v). Then, different concentrations (1.0%, 5.0%, and 10% w/w) of Fe_xO_y-NPs were dispersed in the dope solution using an ultrasound bath for 2 h (Ultrasounds, J.P Selecta, S.A., Barcelona, Spain at 100 W sonication power and 50 Hz frequency). Afterward, 10 mL dope solution was electrospun using a laboratory-scale ES machine (BioInicia, Fluidnatek LE-50 setup, Valencia, Spain). The voltage was adjusted to 12 kV, the needle was placed 13 cm from a rotating drum collector (which was rotating at 200 rpm) and the feed rate was kept constant at 0.9 mL/h. The electrospun PCL/Fe_xO_y nanofibers were then allowed to dry at room temperature, peeled off carefully, and kept in a desiccator for further use and characterization.

3 | CHARACTERIZATION TECHNIQUES

3.1 | Physicochemical properties

3.1.1 | Water contact angle

To determine the WCA for the different electrospun nanofibrous membranes (neat PCL, PCL/GMIONPs, and PCL/CMIONPs nanofiber membranes), an Optical Tensiometer (Attension TL100, KSV, Helsinki, Finland) was used. For the evaluation of the hydrophobicity of nanofiber surfaces, a static measurement of the WCA was conducted. Using a μ-syringe, distilled water drops (1 drop ≈ 2 μL, Milli-Q grade water drop) were injected onto a horizontally leveled membrane (10×10 mm) for 20 s at a rate of 12 F/s (frames per second). The WCA was performed on both sides of the water drop to ensure symmetry and horizontal leveling. Frames with a difference of more than 2° on either side of the center of the frame were rejected. A maximum of five tests were conducted on each sample to ensure reproducibility.

3.1.2 | Water vapor permeability

The water vapor property of the different membranes was measured according to ASTM E96 (ASTM, 2010),[51] which has been described in a previous study.[52] Accordingly, water vapor permeability (WVP, g $h^{-1}{\cdot}m^{-1}$ $Pa^{-1} \times 10^{-7}$) was calculated from Equation (1) as follows:

$$\mathrm{WVP} = P \times t = \frac{\mathrm{WVTR}}{\Delta p} \times t = \frac{\alpha}{\mathrm{AS}(\mathrm{RH}_1 - \mathrm{RH}_2)} \times t, \quad (1)$$

where P is the permeance (the degree to which the membrane admits a flow of water vapor, $g{\cdot}h^{-1}{\cdot}m^{-2}{\cdot}Pa^{-1}$), WVTR (α/A) is the water vapor transmission rate (the amount of water vapor transmitted through the membrane, $g{\cdot}h^{-1}{\cdot}m^{-2}$), α, which can be obtained from the straight line slope, is the vapor flowrate ($g{\cdot}h^{-1}$), A is the permeation area in m^2, $\Delta p = S(\mathrm{RH}_1 - \mathrm{RH}_2)$ is the gradient of water vapor (expressed in Pa) between water-exposed surface (with relative humidity $\mathrm{RH}_1 = 1$) and chamber-exposed surface (with relative humidity $\mathrm{RH}_2 = 0$), where $S = 2646$ Pa and t is the membrane thickness expressed in m units.

3.1.3 | Optical properties

Brightness and color determination

Brightness and color measurements were performed with a portable spectrophotometer (SPECTROPHOTOMETER CM-700d, KONICA MINOLTA SENSING, INC., Tokyo, Japan), which is an instrument designed to measure the color of contact-type objects reflected at visible and near-visible wavelengths (e.g., 360–740 nm).[53] Color transitions from dark to light are expressed by 3 coordinates (L*, ±a*, and ± b*) created by the CIE (Commission Internationale de l'Éclairage, 1976).[54] Thus, L* = 0 indicates diffuse black, and L* = 100 indicates higher specular diffuse white. The

coordinate ±a* indicates the range diffused between red and green, where +a* indicates the red color and −a* indicates green. The coordinate ±b* indicates the range diffused between yellow and blue, where +a* indicates the diffused yellow and −b* indicates the diffused blue.

Light transmission and transparency

Transparency is one of the most attractive characteristics of the different nanofibrous membranes, which prevent light transmission while allowing visibility through the packaging material. An opaque membrane absorbs a significant amount of light. The optical properties of nanofiber membranes were assessed using a UV–vis spectrophotometer (Model 8451A, Hewlett Packard Co., USA) following the guidelines of a previous publication.[49] Briefly, the absorbance values of nanofiber membranes (1×2 cm^2) were recorded at 600 nm and then converted to transmittance using the Lambert–Beer law. The results were presented as transmittance percentage ($T_{600}\%$), and then the transparency (T) of each nanofiber membrane was obtained from Equation (2) as follows[55]:

$$\mathrm{T} = \frac{-\mathrm{Log}T_{600}}{t}, \tag{2}$$

where T_{600} is the transmittance fraction, which indicates how much light is transmitted through the system, and t is the thickness of the membrane (mm). Transparency increases as light transmittance across the membrane decreases, resulting in higher opaqueness.

UV–visible and gap energy

UV–visible absorption spectra were recorded on the nanofibrous membranes to confirm the incorporation of nanoparticles and calculate their gap energies using a UV-spectrophotometer (Varian Cary 6000i, USA). The UV–vis analysis provides an indirect measurement of absorbance and the determination of optical gaps or gap energy (E_g, eV) of samples, as detailed in a previous study.[50] In brief, E_g was extracted using Tauc's relation illustrated in Equation (3):

$$\alpha = \frac{B\left(h\nu - E_g\right)^n}{h\nu}, \tag{3}$$

where α represents the dimensionless absorption coefficient, which was calculated from Equation (4):

$$\alpha = \frac{(1-R)^2}{1-R^2}, \tag{4}$$

and E_g is the optical gap energy (eV) with a transition nature depending on the n value: for direct and indirect allowed transition, n takes ½ and 2 respectively; for direct and indirect forbidden transition, n takes 3/2 and 3 respectively. h is Planck's constant, ν is the frequency, B is a material-dependent constant whose dimensions depend on the value of n ($B = 1$), and R is the reflectance.[56]

3.2 | Mechanical properties

The static tensile test and mechanical parameters of the nanofibrous membranes were conducted according to a slight modification of the standard ISO 527-3:2019.[57] The different parameters, including ultimate tensile strength or maximum stress (UTS or σmax, MPa), elongation or strain at break (εmax, mm/mm), and Young's modulus (MPa) were calculated during this test as described in a previous study.[52]

3.3 | Morphological properties

3.3.1 | Scanning electron microscopy

Scanning electron microscopy (SEM) imaging was used to assess the morphological and microstructural properties of nanofiber membranes. The specimens were observed using a Zeiss EVO microscope (Pleasanton, CA, USA) with an acceleration voltage of 10 kV and a magnification of 3000×.[58] The samples were coated with a thin gold layer to improve their conductivity, as well as the micrograph quality. Thereafter, the membrane thickness was measured with ImageJ free software (1.53q; National Institutes of Health, Bethesda, Maryland, USA).

3.3.2 | Transmission electron microscopy

The transmission electron microscopy (TEM) study was used to gather the elemental information and composition of nanofibers, as well as the nanoparticle distribution within nanofibers. It was performed at 200 kV with a Talos S200 microscope (Field Electron and Ion Company, FEI, USA). Further elemental information on the nanofibers was obtained through ImageJ free software labeling.

3.3.3 | Confocal microscopy

The surface roughness profile was evaluated using a Confocal-Interferometric Optical Microscope (Sensofar S-NEOX, Sky Tech, Bukit Batok, Singapore) employing a Robust Gaussian filter at 100× magnification and 8 μm

amplitude (ISO 4287).[59] Generally, surface roughness is determined by either the centerline average of the surface irregularities or by measuring the distance between their lowest and highest points. In this way, two roughness parameters were calculated: roughness average (*Ra*), which is the arithmetic average of the absolute value of the profile height deviations over the mean length, and quadratic roughness (*Rq* or RMS), which is the root mean square average of the profile height deviation over the mean length. The images were further assessed with ImageJ free software.

3.4 | Functional properties (antioxidant activity)

The antioxidant activity of the nanofiber membranes was tested as described in a previous study.[49] Briefly, 1 mL of each ES dope was mixed with 1 mL of DPPH solution (dissolved in methanol, 40 ppm) and then, the mixture was shaken and incubated for 30 min at 25°C. The absorbance of the samples was recorded at 517 nm using a spectrophotometer. Gallic acid was used as a positive control and the DPPH inhibition (IP%) was calculated according to Equation (5).

$$\mathrm{IP}\,(\%) = \left(\frac{A-B}{A}\right) \times 100, \tag{5}$$

where *A* presents the DPPH absorbance without ES dope and B presents the DPPH absorbance after mixing with ES dope.

3.5 | Statistical analysis

A minimum of three measurements were conducted for each sample. The results were summarized as a mean value and standard deviation (M ± SD) using IBM SPSS software (IBM SPSS Statistics 26.0). Further significant differences ($p < 0.05$) were determined by using a one-way ANOVA at a 95% confidence level.

4 | RESULTS

4.1 | Physicochemical properties

4.1.1 | Water contact angle

The WCA is an integral aspect of many everyday applications, including food packaging, medicine, electronics, and painting. Thus, WCA provides good indications of the surface product wettability or hydrophobicity and of the efficiency of the process.[55] According to WCA values, hydrophilicity, and hydrophobicity are determined by the angle inside a drop in contact with a film surface (hydrophilic surface < 90° < hydrophobic surface), and the increase in this angle indicates a higher degree of hydrophobicity.[55,60] Figure 1 shows the WCA values of neat PCL and composite membranes (PCL/GMIONPs and PCL/CMIONPs, respectively), and Table 1 provides the mean WCA values of each system. The measured WCA value for the neat PCL (118.9 ± 0.8°) was consistent with its hydrophobic properties. The hydrophobic property of PCL is attributed to the presence of CH_2 groups in the main chain of the polymer.[61] This result resembles the previously reported WCA values of PCL electrospun fibers prepared in various solvent systems. For example, the WCA value of electrospun PCL (12% w/v in a mixture of acetic acid: formic acid 3:7) was 118°.[62]

Those systems of PCL with iron oxide nanoparticles exhibited an increase in WCA by increasing the nanoparticle concentration (1%, 5%, and 10%), leading to values of 123.3 ± 0.1, 127.5 ± 0.7, and 132.8 ± 1.5° for PCL/GMIONPs and to 118.4 ± 0.5, 123.0 ± 0.1, and 124.2 ± 0° for PCL/CMIONPs, respectively. The increased hydrophobicity of iron nanoparticles is evidenced by the formation of a crosslinked complex with macromolecules through different interactions, including hydrophobic interactions, hydrogen bonds, and ionic bonds.[63] The presence of hydrophobic nanoparticles on the surface of membranes has been reported to increase their WCAs.[60] A further contributing factor is an increase in surface roughness caused by nanoparticles, which enhances the chemical effect of MIONPs on the hydrophobicity of the composite membranes, in accordance with previous studies.[64] These findings are consistent with previous studies.[65–69]

4.1.2 | Water vapor permeability

It is of paramount importance to determine the WVP of many materials, such as plastic films and membranes, paper, and other sheet materials from which product packages are made. Maintaining the quality of a product in regions with diverse environmental conditions requires an understanding and control of the water vapor transmission rate (WVTR). Through WVTR measurements, the MIONPs were evaluated for their effect on the PCL membranes. Table 1 also summarizes the results of WVTR, permeance, and WVP values. These parameters were reduced significantly when both GMIONPs and CMIONPs were included.

The mean WVP of the neat PCL nanofibers was reduced by about 10%–38% with the incorporation of

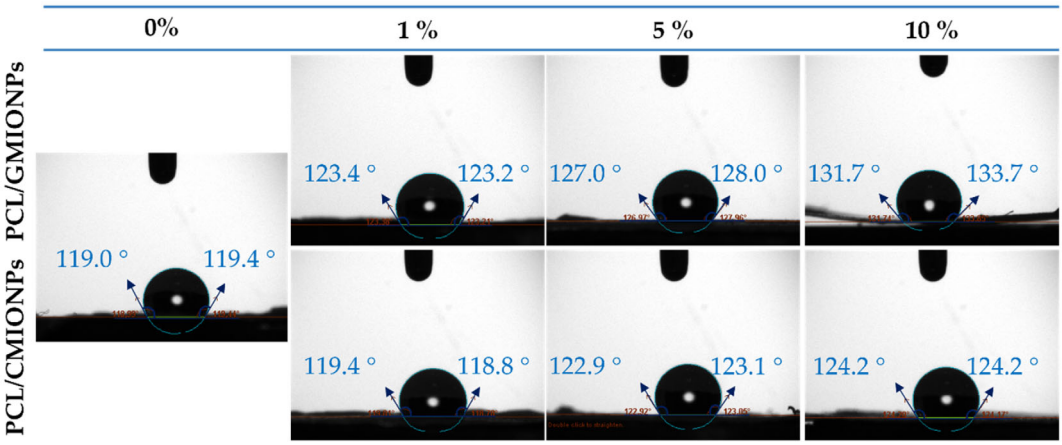

FIGURE 1 Water contact angle profile of PCL/GMIONPs and PCL/CMIONPs nanofibrous membranes (PCL blended with green and chemical iron oxide nanoparticles, respectively, at different concentrations: 0, 1, 5, and 10% w/w). PCL nanofibrous membrane without any MIONPS (0%) was included as a reference system. [Color figure can be viewed at wileyonlinelibrary.com]

TABLE 1 Physicochemical values of PCL/GMIONPs and PCL/CMIONPs nanofibrous membranes (PCL blended with green and chemical iron oxide nanoparticles, respectively, at different concentrations: 0%, 1%, 5%, and 10% w/w).

Sample	C% (w/w)	WCA (°)	WVTR ($g \cdot h^{-1} \cdot m^{-2}$)	Permeance ($g \cdot h^{-1} \cdot m^{-2} \cdot Pa$) $\times 10^{-2}$	WVP ($g \cdot h^{-1} \cdot m^{-2} \cdot Pa^{-1}$) $\times 10^{-7}$
Neat PCL	0%	118.9 ± 0.8^{f}	114.0 ± 0.3^{a}	4.31 ± 0.01^{a}	9.01 ± 0.04^{a}
PCL/GMIONPs	1%	123.3 ± 0.1^{d}	103.9 ± 0.6^{c}	3.93 ± 0.01^{c}	8.29 ± 0.04^{d}
	5%	127.5 ± 0.7^{b}	90.7 ± 0.4^{e}	3.43 ± 0.01^{e}	7.93 ± 0.03^{e}
	10%	132.8 ± 1.5^{a}	82.9 ± 0.7^{f}	3.13 ± 0.01^{f}	7.82 ± 0.03^{f}
PCL/CMIONPs	1%	118.4 ± 0.5^{f}	106.2 ± 0.7^{b}	4.01 ± 0.01^{b}	8.76 ± 0.04^{b}
	5%	123.0 ± 0.1^{e}	101.0 ± 0.3^{d}	3.82 ± 0.01^{d}	8.72 ± 0.02^{b}
	10%	124.2 ± 0^{c}	90.7 ± 0.5^{e}	3.43 ± 0.01^{e}	8.65 ± 0.03^{c}

Note: Different superscript letters (a–f) of each column indicate heterogeneity of variances ($p < 0.05$). PCL nanofibrous membrane without any MIONPS (0%) was included as a reference system.

GMIONPs, and by 7%–26% with CMIONPs incorporation, compared to the WVP of the neat PCL nanofibers (Table 1). This could be due to the formation of well-connected three-dimensional structures[70] and the generation of twisted pathways within the polymer matrix, which blocks and delays water molecules from crossing the matrix.[38] Furthermore, the nanoparticle dispersion restricts the movement of protein chains, thereby inhibiting water infiltration.[69,71] The filler's hydrophobic/hydrophilic balance may be slightly altered by changing the cation. This is mainly due to nanoparticles exhibiting strong interactions with polymer chains, which may result in the consumption of hydrophilic groups, thereby reducing the transmission of water.[72] Several factors can influence the WVP of composite membranes, which comprise hydrophobicity/hydrophilicity, thickness, roughness, compaction, particle size, crystallinity, distribution, and orientation.[65,73,74] In this way, GMIONPs improved the WVP of the composite PCL membranes further compared to CMIONPs, due to their smaller sizes and higher crystallinity. Nanoparticles with higher crystallinity contribute to the enhancement of membrane crystallinity and hydrophobicity by reducing the free hydroxy groups in the membranes, thereby improving their resistance to moisture and reducing WVP.[34,75] In addition, the orientation of nanoparticles may take place, which may be affected by the homogeneity of the crystal system shown by the nanoparticles. The CMIONPs exhibited elongated agglomerates/aggregates, which can leave behind empty pores, thereby allowing moisture to penetrate. This may reflect the non-availability of the chemical stabilizing agents and the interaction between the different polycrystalline structures.[76]

4.1.3 | Optical properties

Brightness and color determination

Figure 2 depicts photographs of the different samples studied. As can be seen, the PCL membranes with GMIONPs and CMIONPs became darker with increasing nanoparticle concentration. A longer processing time may also lead to darker images. For comparison purposes, it is important to maintain the same processing conditions and time for all electrospun membranes. Further analysis of the nanofibrous membranes was conducted using the three CEI coordinates (L*, ±a*, and ±b*) to identify the brightness and color space of the membranes, as summarized in Table 2. A decrease in L* values was observed when the PCL nanofibrous membranes were processed with MIONPs at 5% and 10% (w/w), although without significance at 1% (w/w). An increase in the diffuse red and yellow (+a* and +b*) or decrease in the diffuse green and blue (−a* and −b*) may be related to the nanoparticle type (e.g., Fe_2O_3-NPs, or Fe_3O_4-NPs).[77] Thus, when NPs were progressively incorporated into the PCL nanofibrous membranes, a* was found to vary from −0.06 to 5.36 with GMIONPs (84% Fe_3O_4 and 16% Fe_2O_3), and from −0.06 to 14.94 (Table 2) with CMIONPs (72% Fe_3O_4 and 28% Fe_2O_3).

Similarly, coordinate b* increased with the increase in MIONPs concentration, being higher in PCL/CMIONPs than in PCL/GMIONPs, which may confirm that hematite has a higher proportion in PCL/CMIONPs. Another study reported a similar increase in the (a*, b*) coordinates to (2.95, 7.2) and (3.84, 1.29) when hematite (Fe_2O_3) constituted 14.9% and 15.3% of the total chemical composition, respectively.[77] Nevertheless, color change and other optical properties were further analyzed using UV–vis spectrophotometry.

Light transmission and transparency

Table 2 summarizes the corresponding values for the membrane transmittance ($T_{600}\%$) and transparency (T). The incorporation of MIONPs into the PCL electrospun membranes resulted in a significant decrease in the $T_{600}\%$ and an increase in the T index. Accordingly, the neat PCL exhibited white opaque membranes with the highest transmittance (0.94 ± 0.09%). When it was processed with GMIONPs (1%–10% w/w), the $T_{600}\%$ was

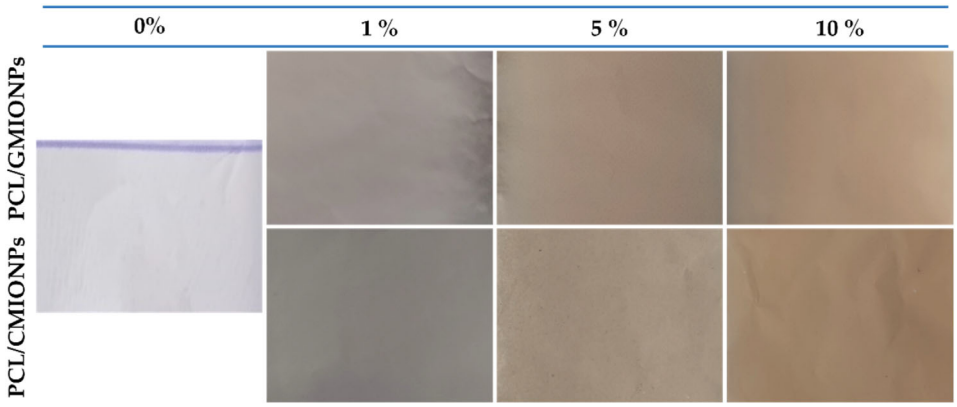

FIGURE 2 Photographs of PCL/GMIONPs and PCL/CMIONPs electrospun nanofibrous membranes (PCL blended with green and chemical iron oxide nanoparticles, respectively, at different concentrations: 0%, 1%, 5%, and 10% w/w). PCL nanofibrous membrane without any MIONPS (0%) was included as a reference system. [Color figure can be viewed at wileyonlinelibrary.com]

TABLE 2 Optical values (CEI coordinates [L*, a*, and b*], light transmission, and gap energy) of PCL/GMIONPs and PCL/CMIONPs nanofibrous membranes (PCL blended with green and chemical iron oxide nanoparticles, respectively, at different concentrations: 1%, 5%, and 10% w/w).

Sample	C% (w/w)	L*	a*	b*	T_{600} (%)	T	E_g (eV)
Neat PCL	0%	90.69 ± 0.25^{a}	-0.06 ± 0.04^{e}	-1.13 ± 0.03^{g}	0.94 ± 0.09^{a}	32.25^{g}	1.29
PCL/GMIONPs	1%	90.42 ± 0.85^{a}	-0.03 ± 0.11^{e}	-0.79 ± 0.28^{f}	0.64 ± 0.09^{b}	34.65^{e}	-
	5%	88.08 ± 0.03^{b}	3.35 ± 0.02^{c}	4.49 ± 0.04^{d}	0.19 ± 0.02^{d}	38.96^{a}	-
	10%	85.29 ± 0.94^{c}	5.36 ± 0.60^{b}	8.97 ± 0.06^{b}	$0.13 \pm 0.0.07^{e}$	38.12^{c}	2.09
PCL/CMIONPs	1%	89.81 ± 0.94^{a}	0.93 ± 0.09^{d}	-0.40 ± 0.19^{e}	0.65 ± 0.02^{b}	33.37f	-
	5%	84.02 ± 0.34^{d}	5.24 ± 0.24^{b}	6.33 ± 0.27^{c}	0.21 ± 0.06^{c}	38.91^{b}	-
	10%	75.75 ± 0.90^{e}	14.94 ± 0.48^{a}	23.11 ± 0.06^{a}	0.14 ± 0.08^{e}	37.34^{d}	1.47

Note: Different superscript letters (a–f) of each column indicate heterogeneity of variances ($p < 0.05$). PCL nanofibrous membrane without any MIONPS (0%) was included as a reference system.

reduced by about 32%–87% by filling up the free space between the nanofibers, where the T value was enhanced by about 7%–17% (Table 2, $p < 0.05$). Lastly, when it was processed with CMIONPs (1%–10% w/w), the observed $T_{600}\%$ was reduced by about 31%–85%, corresponding to 7%–17% of slightly different transparency to the GMIONPs (Table 1). This was attributed to the increase of the crystalline nanoparticles content in the polymer chain, which hinders their mobility. Nanofillers may fill up free spaces in polymer chains by being dispersed into the chains, thereby blocking the passage of light through the membrane. Similar results were found with other polymers blended with different nanoparticles.[36,41,55,78,79]

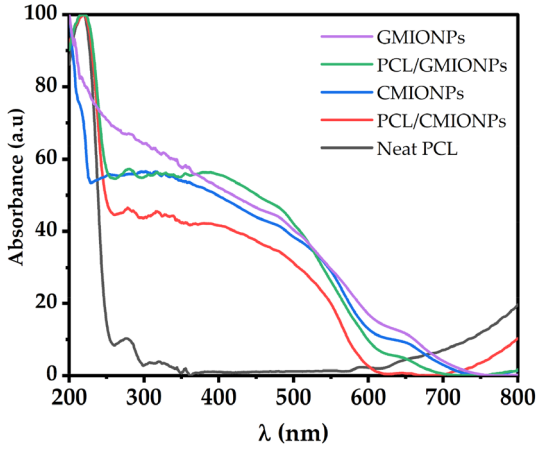

FIGURE 3 UV–visible absorption spectra of PCL/GMIONPs and PCL/CMIONPs membranes (PCL blended with green and chemical iron oxide nanoparticles, respectively, at (10% w/w). GMIONPs, CMIONPs, and PCL nanofibrous membranes without any MIONPS were included as reference systems. [Color figure can be viewed at wileyonlinelibrary.com]

UV–visible and gap energy: As shown in Figure 3, the comparison between the spectra of the pure PCL membrane with those of PCL and MIONPs based membranes clearly reflects the contribution of MIONPs, which lead to a remarkable enhancement of the absorption band in the UV–visible spectrum. In addition to the enhanced absorption band recorded at around 274 nm for both GMIONPs and CMIONPs, which increased by about 82% and 78%, respectively, they recorded broad absorption bands throughout the entire spectral range, particularly up to approximately 700 and 610 nm for the spectra on GMIONPs and CMIONPs, respectively.

Furthermore, the corresponding direct band gap for each spectrum was determined to be increased by the presence of MIONPs; thus, the neat PCL showed a small gap energy (1.29 eV, Table 2), whereas the gap energies of PCL/GMIONPs and PCL/CMIONPs increased to 2.09 and 1.47 eV, in the order already mentioned. Incidentally, the direct gap energies of the isolated MIONPs were found to be 2.94 eV for the GMIONPs and 2.19 eV for the CMIONPs. This was due to the increase in Fe_3O_4 proportion, as well as the smaller size and higher crystallinity, as reported elsewhere.[80] MIONPs represent the most significant absorption of visible light with direct and indirect band gaps of 1.6–3.01 eV, which cover most of the visible spectrum.[56,80,81]

4.2 | Mechanical properties

Figure 4a illustrates the tensile profile of PCL-based membranes, neat PCL, and PCL with 10% w/w of GMIONPs or CMIONPs. To facilitate better visualization, the tensile profile of PCL/GMIONPs and PCL/CMIONPs was included in Figure 4b,c. The mechanical properties

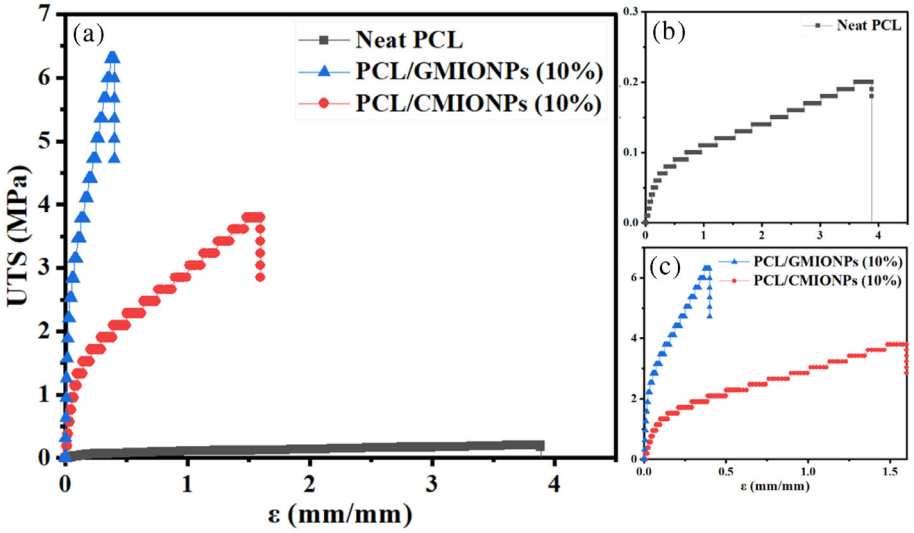

FIGURE 4 Tensile test profile of PCL/GMIONPs and PCL/CMIONPs membranes (PCL blended with green and chemical iron oxide nanoparticles, respectively, at 10% w/w). PCL nanofibers without any MIONPS were included as a reference system. [Color figure can be viewed at wileyonlinelibrary.com]

are summarized in Table 3. As expected, the neat PCL exhibited a shorter elastic area followed by a longer elongation area. In contrast, PCL/GMIONPS and PCL/CMIONPs nanofibrous membranes show higher values for Young's modulus (MPa) and the maximum stress (σ_{max}, MPa) with a shorter plastic region as compared to the neat PCL membrane. Young's modulus increased by about 99% and 97% and σ_{max} increased by about 97% and 94% over the value corresponding to the neat PCL membranes. Similar studies have found similar increases in these parameters.[82] The incorporation of immiscible nanoparticles may favor the formation of hydrogen bonding with NPs giving rise to non-homogeneous networks within the fibers that may be responsible for the enhancement of the mechanical properties of the polymeric membranes.[41,83] However, higher concentrations of larger nanoparticles can lead to agglomeration of nanoparticles in/on the fiber by forming beads, which can restrict the mechanical properties.

Furthermore, a remarkable decrease in the strain at break (ε_{max}) was observed when the PCL was reinforced with MOINPs, which indicates that the presence of solid material within PCL nanofibers may indurate the membrane by increasing the thickness and reducing the cohesion forces within the fibers.[41,84] The nanoparticles' type and size may contribute to this behavior. Therefore, the smaller crystalline sizes led to stronger networks between the nanoparticles and the polymer through the improvement of the interactions within the polymer structure, resulting in improved mechanical properties. Similar results with respect to the mechanical properties of polymers with nanoparticles have been previously reported, which may also be attributed to the type and size of nanoparticle interconnections.[49,85] Prior studies have reported similar results regarding the mechanical properties of polymers containing nanoparticles.[86–88]

4.3 | Morphological properties

4.3.1 | Confocal microscopy: Roughness

The roughness of the membrane surfaces is a crucial parameter for the growth and adherence of the lines of different cells for biomaterial purposes. 3D surface plots of the neat PCL, PCL/GMIONPs, and PCL/CMIONPs nanofibrous membranes are depicted in Figure 5. Roughness results (*Ra* and *Rq*) are summarized in Table 4. Accordingly, increases in *Ra* and *Rq* were observed when the PCL electrospun membrane was processed with both nanoparticle types. Nevertheless, *Ra* and *Rq* values (in nanometers) of PCL/CMIONPs were greater than

TABLE 3 Results of the mechanical parameters of PCL/GMIONPs and PCL/CMIONPs nanofibrous membranes (PCL blended with green and chemical iron oxide nanoparticles, respectively; concentration = 10% w/w).

Sample	C% (w/w)	Young's modulus (MPa)	σ_{max} (MPa)	ε_{max} (mm/mm)
Neat PCL	0%	0.3 ± 0.1^{c}	0.2 ± 0.1^{c}	3.9 ± 0.9^{a}
PCL/GMIONPs	10%	87.6 ± 1.8^{a}	6.3 ± 0.1^{a}	0.4 ± 0.1^{c}
PCL/CMIONPs	10%	15.8 ± 1.1^{b}	3.8 ± 0.2^{b}	1.6 ± 0.3^{b}

Note: Different superscript letters (a-b) of each column indicate heterogeneity of variances ($p < 0.05$). PCL nanofibrous membrane without any MIONPS (0%) was included as a reference system.

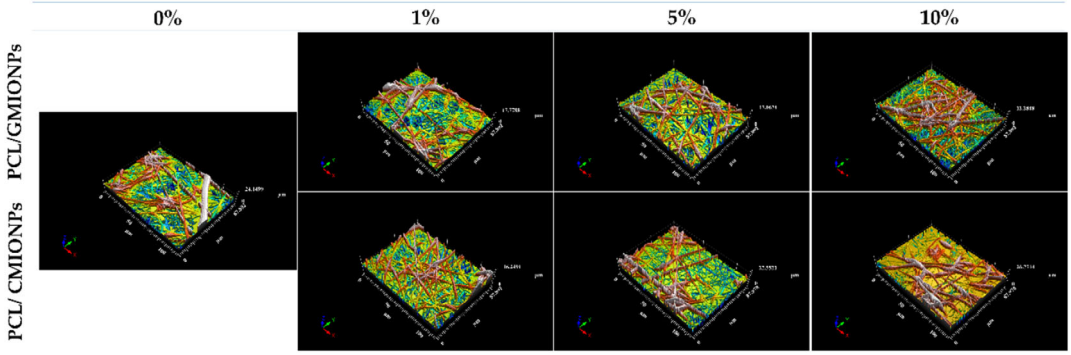

FIGURE 5 3D surface plot of PCL/GMIONPs and PCL/CMIONPs nanofibrous membranes (PCL blended with green and chemical iron oxide nanoparticles, respectively, at different concentrations: 0%, 1%, 5%, and 10% w/w). A 3D surface plot of PCL nanofibrous membrane without any MIONPS (0%) was included as a reference. [Color figure can be viewed at wileyonlinelibrary.com]

TABLE 4 Results for membrane average roughness (*Ra*), quadratic average roughness (*Rq*), thickness (μm), nanofiber diameter (nm), of PCL/GMIONPs and PCL/CMIONPs (PCL blended with green and chemical iron oxide nanoparticles, respectively, at different concentrations: 0%, 1%, 5%, and 10% w/w).

Sample	C% (w/w)	*Ra* (nm)	*Rq* (nm)	Membrane thickness (μm)	Nanofiber diameter (nm)
Neat PCL	0%	27.6 ± 2.8^{f}	34.2 ± 3.3^{g}	62.7 ± 0.3^{f}	252 ± 109
PCL/GMIONPs	1%	33.4 ± 2.1^{e}	42.7 ± 1.3^{f}	63.3 ± 0.3^{e}	258 ± 124
	5%	56.7 ± 3.6^{c}	73.3 ± 2.1^{d}	69.4 ± 0.3^{b}	366 ± 197
	10%	91.2 ± 1.2^{a}	107.7 ± 2.6^{c}	74.9 ± 0.3^{a}	348 ± 180
PCL/CMIONPs	1%	44.6 ± 1.4^{d}	63.2 ± 2.1^{e}	65.5 ± 0.3^{d}	314 ± 118
	5%	86.0 ± 2.1^{b}	114.8 ± 1.7^{b}	68.5 ± 0.2^{c}	388 ± 191
	10%	91.1 ± 1.8^{a}	135.2 ± 1.3^{a}	75.7 ± 0.3^{a}	506 ± 158

Note: Different superscript letters (a–g) of each column indicate heterogeneity of variances ($p < 0.05$). Results for PCL nanofibrous membrane without any MIONPS (0%) were included as a reference system.

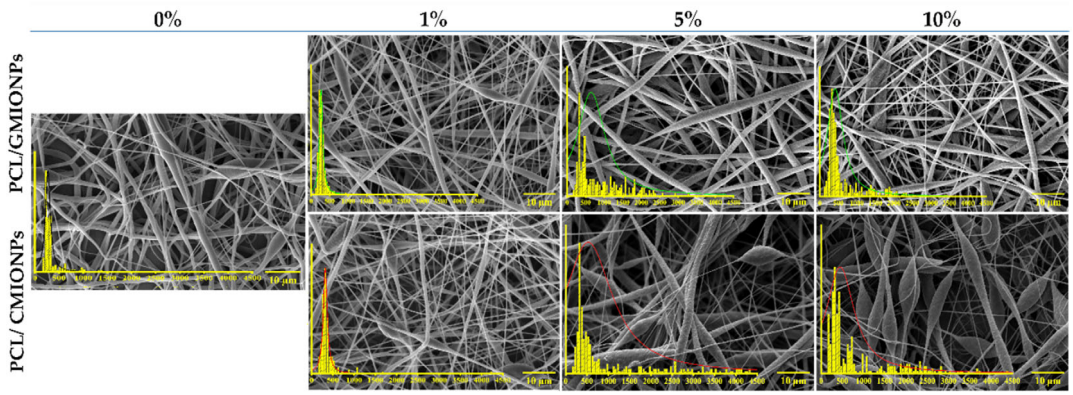

FIGURE 6 Scanning electron microscopy (SEM) images of PCL/GMIONPs and PCL/CMIONPs electrospun nanofibrous membranes (PCL blended with green and chemical iron oxide nanoparticles, respectively, at different concentrations: 0%, 1%, 5%, and 10% w/w). The SEM image of the PCL nanofibrous membrane without any MIONPS (0%) was included as a reference system. [Color figure can be viewed at wileyonlinelibrary.com]

PCL/GMIONPs, which is probably due to the sizes of the nanoparticles. Thus, the average size of CMIONPs in this study was ≈24 nm. In addition, the nanoparticles' shapes seemed to be elongated, with different orientations, as seen in the TEM analysis. These results are in line with those of SEM and TEM analyses. Similar altered structures have been found in other studies.[89,90]

4.3.2 | Scanning electron microscopy

The morphologies of electrospun nanofibers from solutions of PCL, PCL/GMIONPs, or PCL/CMIONPs, along with their respective fiber diameter distributions, are depicted in Figure 6. Smooth and homogeneous nanofibers were observed in the neat PCL membranes. In contrast, the incorporation of MIONPs modified the nanofiber surface by producing irregularities and roughness. This may be attributed to the different properties contributed by nanoparticles on/within fiber surfaces during the ES process (e.g., granulation, dispersion, agglomeration).[55,65] An increase in GMIONPs or CMIONPs content led to a change from smooth fiber surfaces (0%) to rough fiber surfaces, which was particularly evident for MIONPs concentrations of 5% and 10%. This increase in MIONPs content also leads to an increase in fiber broadening zones, in particular with CMIONPs, as well as to a greater dispersion of fiber diameters, with minor aggregation knots, which became larger with the increase of nanoparticle concentration. Larger aggregates of nanoparticles have also been reported in systems with higher nanoparticle concentrations.[91] An increase in GMIONPs or CMIONPs concentration also led to an increase in the average diameter of the nanofibers (Table 4). Similar findings have been reported elsewhere.[92]

4.3.3 | Transmission electron microscopy

The nanofiber morphologies of the neat PCL and PCL with GMIONPs or CMIONPs, as well as their diameter distributions, are depicted in Figure 7. In general, the nanoparticles were observed to be uniformly distributed, with some aggregation/agglomeration. Nevertheless, the GMIONPs seemed slightly aggregated/agglomerated, which could be a result of the interactions between the phenolic compound charges on the GMIONPs surfaces and the polymer chains within the fiber, changing their structures.[89,90] In addition, as the metal oxide nanoparticle content increased, aggregations became larger.[91] In this regard, increasing the surface roughness of polymer surfaces is crucial, since it can either facilitate or interfere with macromolecule adsorption and membrane formation.[93] Roughness measurements were further assessed, and they are discussed in the next section.

4.4 | Functional properties (antioxidant activity)

The antioxidant activities of the neat PCL and PCL with GMIONPs or CMIONPs membranes were evaluated by measuring the inhibition of DPPH (IP%), as is shown in Figure 8. Additionally, an IP% of 95% was obtained with gallic acid as a positive control. An increase in IP% was observed in the presence of MIONPs, due to the antioxidant properties of these nanoparticles, which may have beneficial effects on a variety of systems.[41,94] Regarding the different MINPs, the GMIONPs increased the IP% of neat PCL from 20.8% to 58.1%, 85.5%, and 94.0% when they were added at different concentrations (1, 5, and 10 wt%, respectively). Meanwhile, the CMIONPs increased the IP% of neat PCL from 20.8% to 24.5%, 30.5R, and 39.2% with the incorporation of 1, 5, and 10 wt%, respectively. The increase in IP% in the presence of GMIONPs to almost that of commercial gallic acid (IP % = 95%) was attributed to the presence of higher concentrations of polyphenolic reactive oxygen species (ROS like H_2O_2, O_2–, $_1O^2$, –OH), which act as antioxidants.[49] In this study, the GMIONPs (1 wt%) exhibited higher antioxidant activity (IP% = 58.1%, Table 4) than CMIONPs (10 wt%), which exhibited an IP% of 39.2%, Table 1. The lower antioxidant activity of CMIONPs membranes as compared to GMIONPs membranes indicates the non-availability of the reducing agent in the chemical synthesis.[76] A study elsewhere has reported an

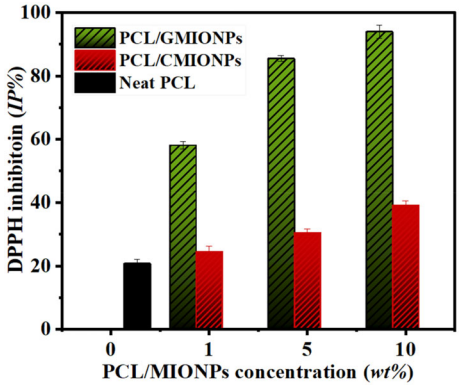

FIGURE 8 Antioxidant activity (DPPH inhibition IP%) of PCL/GMIONPs and PCL/CMIONPs nanofibrous membranes (PCL blended with green and chemical iron oxide nanoparticles, respectively, at different concentrations: 0%, 1%, 5%, and 10% w/w). [Color figure can be viewed at wileyonlinelibrary.com]

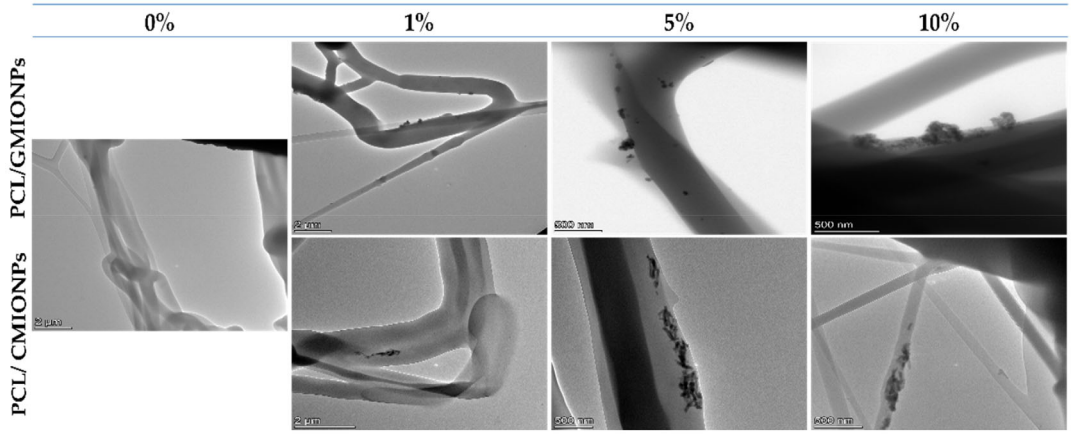

FIGURE 7 Transmission electron microscopy (TEM) images of fibers from PCL/GMIONPs and PCL/CMIONPs nanofibrous membranes (PCL blended with green and chemical iron oxide nanoparticles, respectively, at different concentrations: 0%, 1%, 5%, and 10% w/w). An image of fibers from the PCL nanofibrous membrane without any MIONPS (0%) was included as a reference. [Color figure can be viewed at wileyonlinelibrary.com]

IP% of 55.1% for chemical iron oxide nanoparticles incorporated into another polymer at 20 wt%.[41] Therefore, the antioxidant capacity of GMIONPs may be beneficial to the antimicrobial property, which has already been demonstrated in previous research.[49]

Nevertheless, comparing the antioxidant activity evaluation methods used in our study, which measured the inhibition of DPPH (IP%), with other commonly employed methods, is crucial for assessing their strengths and limitations. The DPPH assay is a widely used method for evaluating antioxidant activity by measuring the ability of a sample to scavenge DPPH free radicals.[95] In our study, we utilized this assay to assess the antioxidant capacity of PCL membranes with GMIONPs and CMIONPs. While the DPPH assay offers a direct and rapid assessment of antioxidant activity, it is important to acknowledge that different methods may yield varying results due to differences in chemical environments and reaction mechanisms. Alternative methods for evaluating antioxidant activity include the Trolox equivalent antioxidant capacity (TEAC) assay, ferric reducing antioxidant power (FRAP) assay, hydroxyl radical scavenging capacity (HOSC), and oxygen radical absorbance capacity (ORAC) assay, among others. These methods employ different principles, such as electron transfer or hydrogen atom transfer, to measure antioxidant capacity.[96]

For example, a study by Reis et al.[97] investigated the antioxidant behavior of extract-loaded polymer-NPs based on different polymer types. The antioxidant activity of the extract-loaded polymer-NPs varied depending on the polymer type, as evaluated using the DPPH and TEAC methods. When comparing the antioxidant activity of the extract-loaded poly(lactic-co-glycolic acid) (PLGA) with the free extract, a decrease in antioxidant activity was observed in the extract-loaded PLGA. The antioxidant activity of the extract-loaded PLGA (≈0.5%) was lower than that of the free extract (≈80%), but higher than the PLGA alone (negligible). In contrast, the extract-loaded PCL exhibited an increase in antioxidant activity (≈6%) compared to PCL alone. Interestingly, when evaluating the extract-loaded polymer-NPs under different pH conditions (5.5 and 7.4), the antioxidant activity significantly increased, particularly at acidic pH 5.5, with approximately 15% and 14.9% improvement for extract-loaded PLGA and PCL, respectively. Furthermore, when comparing the TEAC values, the extract-loaded PLGA NPs showed lower values compared to PLGA NPs alone, suggesting potential retention or degradation of the antioxidant compounds. Conversely, the extract-loaded PCL NPs demonstrated an increase in TEAC compared to PCL NPs alone, indicating improved antioxidant activity after incorporation.[97] These results highlight the significant influence of the polymer choice and experimental conditions on the antioxidant behavior of the NPs, with PCL NPs showing promise for enhancing the antioxidant properties of the composite system.

To comprehensively compare the antioxidant activity of GMIONPs and CMIONPs with other methods, further studies utilizing these alternative assays would be valuable. Such comparisons would enhance our understanding of the effectiveness and potential advantages of GMIONPs as antioxidants, enabling meaningful comparisons with existing literature.

5 | CONCLUSIONS

The incorporation of MIONPs into PCL-based electrospun membranes has the potential to enhance their properties in several ways. An enhancement in the membrane hydrophobicity and water solubility was confirmed through WCA measurements, as well as a reduction in WVP. The incorporation of both types of MIONPs contributed to the color change of the electrospun membranes and enhanced gap energy and opacity by blocking the light from traversing through the membrane. Furthermore, the mechanical properties and antioxidant activity of the membranes containing PCL and MIONPs were more adequate with the green MIONPs than with the chemical MIONPs. The increase in the surface roughness of polymer surfaces with MIONPs may be regarded as a key factor since it can either facilitate or interfere with macromolecule adsorption and membrane formation. Additionally, the numerical results demonstrate the impact of MIONPs on various properties of the membranes:

1. Water barrier properties:
   - Incorporating 10% GMIONPs and CMIONPs increased the WCA to 132.8 ± 1.5 and $124.2 \pm 0°$, respectively, indicating enhanced hydrophobicity.
   - The water vapor transmission rate (WVTR) decreased from 114.0 ± 0.3 to 82.9 ± 0.7 and 90.7 ± 0.5 $g \cdot h^{-1} \cdot m^{-2}$ with 10% GMIONPs and CMIONPs, respectively, suggesting improved water barrier performance.
   - The WVP also decreased from 9.01 ± 0.04 to 7.82 ± 0.03 and 8.65 ± 0.03 $g \cdot h^{-1} \cdot m^{-2} \cdot Pa^{-1} \times 10^{-7}$ with 10% GMIONPs and CMIONPs, respectively, indicating reduced WVP and enhanced water barrier properties.
2. Optical properties:
   - The light transmission ($T_{600\%}$) of membranes with 10% GMIONPs and CMIONPs decreased to $0.13 \pm 0.0.07$ and $0.14 \pm 0.08\%$, respectively, indicating increased opacity.

- The band gap energy (E_g) of membranes with 10% GMIONPs and CMIONPs increased to 2.09 and 1.47 eV, respectively. This suggests an enhancement in semiconducting properties, leading to improved optical characteristics such as increased opacity and reduced light transmission.

3. Mechanical properties:
   - The Young's modulus increased to 87.6 ± 1.8 and 15.8 ± 1.1 MPa with 10% GMIONPs and CMIONPs, respectively, indicating improved stiffness.
   - The maximum stress (σ_{max}) increased to 6.3 ± 0.1 and 3.8 ± 0.2 MPa with 10% GMIONPs and CMIONPs, respectively, indicating enhanced mechanical strength.
   - The elongation (ε_{max}) decreased to 0.4 ± 0.1 and 1.6 ± 0.3 mm/mm with 10% GMIONPs and CMIONPs, respectively, suggesting enhanced flexibility.
4. Morphological properties:
   - The surface roughness (*Ra*) increased to 91.2 ± 1.2 and 91.1 ± 1.8 nm with 10% GMIONPs and CMIONPs, respectively, indicating a rougher membrane surface.
   - The membrane thickness increased to 74.9 ± 0.3 and 75.7 ± 0.3 μm with 10% GMIONPs and CMIONPs, respectively, contributing to the altered morphology.
   - The nanofiber diameter increased to 348 ± 180 and 506 ± 158 nm with 10% GMIONPs and CMIONPs, respectively, further impacting the surface morphology.

In addition, this work reveals that green MIONPs could be used with several advantages, among which the remarkable increase in antioxidant activity is noteworthy. As a result of the incorporation of these nanoparticles, future applications could be significantly enhanced, and toxic waste and costs could be reduced. The development of well-controlled green MIONPs and their dispersion within electrospun nanofibrous membranes may allow their incorporation into sustainable applications that significantly enhance their functional properties. A combination of all the above attributes makes PCL/GMIONPs nanofibrous membranes an excellent choice for several applications, ranging from pharmaceutical biomaterials and biomedical applications to battery fabrication. They may also be used in functional packaging, with functional activity.

AUTHOR CONTRIBUTIONS

Johar Amin Ahmed Abdullah: Conceptualization (lead); data curation (equal); formal analysis (equal); investigation (equal); methodology (equal); software (equal); validation (equal); writing – original draft (equal). **Víctor Perez-Puyana:** Data curation (equal); formal analysis (equal); investigation (equal); methodology (equal); validation (equal); writing – original draft (equal). **Antonio Guerrero:** Conceptualization (equal); project administration (equal); resources (lead); supervision (equal); visualization (equal); writing – review and editing (equal). **Alberto Romero:** Conceptualization (equal); supervision (equal); validation (equal); visualization (equal); writing – review and editing (equal).

ACKNOWLEDGMENTS

This study was financially supported by MCIN/AEI/10.13039/501100011033/FEDER, UE from the Spanish Government (Ref. PID2021-124294OB-C21). The authors gratefully acknowledge the financial support. The authors thank the predoctoral grant from J. A. A. A (Universidad de Sevilla) J. A. A. A. also would like to thank the support from SHA Group represented by Abdul Jabbar Hayel Saeed Anam. In addition, the authors thank the postdoctoral contract of Víctor Manuel Pérez Puyana from the European Social Fund/Junta de Andalucía ("Contratación de Personal Investigador Doctor," PAIDI DOCTOR Convocatoria 2019–2020).

CONFLICT OF INTEREST STATEMENT

There are no conflicts to declare.

DATA AVAILABILITY STATEMENT

The data presented in this study are available on request from the corresponding author.

ORCID

Johar Amin Ahmed Abdullah https://orcid.org/0000-0002-5923-8254

REFERENCES

[1] C. H. T. Yew, P. Azari, J. R. Choi, F. Muhamad, B. Pingguan-Murphy, *Polymers (Basel)* **2018**, *10*, 1387.
[2] P. Rathore, J. D. Schiffman, *ACS Appl. Mater. Interfaces* **2021**, *13*, 48.
[3] A. Mamun, L. Sabantina, M. Klöcker, A. Heide, T. Blachowicz, A. Ehrmann, *Polymers (Basel)* **2022**, *14*, 1.
[4] D. Y. Lee, K. H. Lee, B. Y. Kim, N. I. Cho, *J. Sol-Gel Sci. Technol.* **2010**, *54*, 63.
[5] A. Greiner, J. H. Wendorff, *Angew. Chemie – Int. Ed.* **2007**, *46*, 5670.
[6] K. Klinkhammer, N. Seiler, D. Grafahrend, J. Gerardo-Nava, J. Mey, G. A. Brook, M. Möller, P. D. Dalton, D. Klee, *Tissue Eng Part C Methods* **2009**, *15*, 77.
[7] T. Grothe, D. Wehlage, T. Böhm, A. Remche, A. Ehrmann, *Tekstilec* **2017**, *60*, 290.
[8] F. J. García-Mateos, T. Cordero-Lanzac, R. Berenguer, E. Morallón, D. Cazorla-Amorós, J. Rodríguez-Mirasol, T. Cordero, *Appl. Catal. B Environ.* **2017**, *211*, 18.
[9] F. E. Che Othman, N. Yusof, H. Hasbullah, J. Jaafar, A. F. Ismail, N. Abdullah, N. A. H. Md Nordin, F. Aziz, W. N. Wan Salleh, *J. Ind. Eng. Chem.* **2017**, *51*, 281.
[10] G. T. V. Prabu, B. Dhurai, *Sci. Rep.* **2020**, *10*, 1.

[11] S. Gao, G. Tang, D. Hua, R. Xiong, J. Han, S. Jiang, Q. Zhang, C. Huang, *J. Mater. Chem. B* **2019**, *7*, 709.
[12] A. Mamun, *Tekstilec* **2019**, *62*, 89.
[13] D. Wehlage, H. Blattner, A. Mamun, I. Kutzli, E. Diestelhorst, A. Rattenholl, F. Gudermann, D. Lütkemeyer, A. Ehrmann, *AIMS Bioeng.* **2020**, *7*, 43.
[14] E. Boyraz, F. Yalcinkaya, J. Hruza, J. Maryska, *Materials (Basel)* **2019**, *12*, 1.
[15] T. Kozior, M. Trabelsi, A. Mamun, L. Sabantina, A. Ehrmann, *Polymers (Basel)* **2019**, *11*, 1.
[16] F. Yalcinkaya, E. Boyraz, J. Maryska, K. Kucerova, *Materials (Basel)* **2020**, *13*, 493.
[17] Y. Xue, X. Guo, H. Zhou, J. Zhou, *Carbon N.Y.* **2019**, *154*, 219.
[18] S. Kohn, D. Wehlage, I. J. Junger, A. Ehrmann, *Catalysts* **2019**, *9*, 1.
[19] X. Li, W. Chen, Q. Qian, H. Huang, Y. Chen, Z. Wang, Q. Chen, J. Yang, J. Li, Y. W. Mai, *Adv. Energy Mater.* **2021**, *11*, 2000845.
[20] A. Abutaleb, *Polymers (Basel)* **2021**, *13,* 2290.
[21] C. M. A. Gangemi, M. Iudici, L. Spitaleri, R. Randazzo, M. Gaeta, A. D'Urso, A. Gulino, R. Purrello, M. E. Fragalà, *Molecules* **2019**, *24*, 3344.
[22] R. Contreras-Cáceres, L. Cabeza, G. Perazzoli, A. Díaz, J. M. López-Romero, C. Melguizo, J. Prados, *Nanomaterials* **2019**, *9*, 1.
[23] M. Salmeri, G. Ognibene, L. Saitta, C. Lombardo, C. Genovese, M. Barcellona, A. D'Urso, L. Spitaleri, I. Blanco, G. Cicala, A. Gulino, M. E. Fragalà, *Molecules* **2020**, *25*, 1696.
[24] F. Wang, Z. Xie, J. Liang, B. Fang, Y. Piao, M. Hao, Z. Wang, *Environ. Sci. Technol.* **2019**, *53*, 6989.
[25] J. Ouyang, Z. Zhao, H. Yang, Y. Zhang, A. Tang, *Appl. Clay Sci.* **2018**, *152*, 221.
[26] Y. Piao, Q. Jiang, H. Li, H. Matsumoto, J. Liang, W. Liu, C. Pham-Huu, Y. Liu, F. Wang, W. Liu, F. Wang, *ACS Catal.* **2020**, *10*, 7894.
[27] L. Duque Sánchez, N. Brack, A. Postma, P. J. Pigram, L. Meagher, *Biomaterials* **2016**, *106*, 24.
[28] W. Mao, H. S. Yoo, *Macromol. Biosci.* **2017**, *17*, 1700057.
[29] S. Shahmoradi, F. Yazdian, F. Tabandeh, Z.-S. Soheili, A. S. Hatamian Zarami, M. Navaei-Nigjeh, *Mater. Sci. Eng. C* **2017**, *73*, 300.
[30] V. Perez-Puyana, P. Wieringa, A. Guerrero, A. Romero, L. Moroni, *ACS Appl. Mater. Interfaces* **2021**, *13*, 29293.
[31] A. A. Nwakaudu, N. C. Iheaturu, *Applied Signals Reports* **2015**, *2*, 38.
[32] Y. Wang, Q. Yang, G. Shan, C. Wang, J. Du, S. Wang, Y. Li, X. Chen, X. Jing, Y. Wei, *Mater. Lett.* **2005**, *59*, 3046.
[33] N. Kizildag, *Marmara Univ. J. Sci.* **2015**, *27*, 15.
[34] S. Shankar, L.-F. Wang, J. Rhim, *Food Packag. Shelf Life* **2019**, *21*, 100363.
[35] A. Mohammadi, M. Moradpour, M. Saeidi, A. Karim, *LWT – Food Sci. Technol.* **2014**, *58*, 142.
[36] P. Kanmani, J. W. Rhim, *Food Chem.* **2014**, *148*, 162.
[37] Q. He, Y. Zhang, X. Cai, S. Wang, *Int. J. Biol. Macromol.* **2016**, *84*, 153.
[38] S. Fakhreddin, M. Rezaei, M. Zandi, F. Farahmandghavi, *Food Hydrocolloids* **2015**, *44*, 172.
[39] C. H. C. Flaker, R. V. Lourenço, A. M. Q. B. Bittante, P. J. A. Sobral, *J. Food Eng.* **2015**, *167*, 65.
[40] S. Sahraee, J. M. Milani, B. Ghanbarzadeh, H. Hamishehkar, *Int. J. Biol. Macromol.* **2017**, *97*, 373.
[41] Z. Mehmood, M. B. Sadiq, M. R. Khan, *J. Food Saf.* **2020**, *40*, e12814.
[42] N. Tran, A. Mir, D. Mallik, A. Sinha, S. Nayar, T. J. Webster, *Int. J. Nanomed.* **2010**, *5*, 277.
[43] A. Azam, A. S. Ahmed, M. Oves, M. S. Khan, S. S. Habib, A. Memic, *Int. J. Nanomed.* **2012**, *7*, 6003.
[44] N. Singh, G. J. S. Jenkins, R. Asadi, S. H. Doak, *Nano Rev.* **2010**, *1*, 5358.
[45] N. Faria, D. Pereira, B. Mergler, J. Powell, A. Synthesis. 2011 11th IEEE International Conference on Nanotechnology; IEEE, 2011. pp. 837.
[46] P. Mukherjee, A. Ahmad, D. Mandal, S. Senapati, S. R. Sainkar, M. I. Khan, R. Parishcha, P. V. Ajaykumar, M. Alam, R. Kumar, M. Sastry, *Nano Lett.* **2001**, *1*, 515.
[47] A. Rufus, N. Sreeju, V. Vilas, D. Philip, *J. Mol. Liq.* **2017**, *242*, 537.
[48] J. A. A. Abdullah, M. Jiménez-Rosado, V. Perez-Puyana, A. Guerrero, A. Romero, *Nanomaterials* **2022**, *12*, 2449.
[49] J. A. A. Abdullah, M. Jiménez-Rosado, A. Guerrero, A. Romero, *Materials (Basel)* **1966**, *2022*, 15.
[50] J. A. A. Abdullah, L. Salah Eddine, B. Abderrhmane, M. Alonso-González, A. Guerrero, A. Romero, J. A. Ahmed, L. Salah, B. Abderrhmane, *Sustain. Chem. Pharm.* **2020**, *17*, 100280.
[51] ASTEM E96/E96M-10, Standard Test Methods for Water Vapor Transmission of Materials, ASTM International, West Conshohocken, PA, **2010**, Book of Standards Volume: 04.06, 12. https://doi.org/10.1520/E0096_E0096M-10
[52] J. A. A. Abdullah, M. Jiménez-Rosado, J. J. Benítez, A. Guerrero, A. Romero, *Polymers (Basel)* **2022**, *14*, 4487.
[53] P. Sanmartín, M. Gambino, E. Fuentes, M. Serrano, *Sensors (Switzerland)* **2020**, *20*, 2348.
[54] M. D. Fairchild, Color Appearance Models, John Wiley & Sons, Ltd., New Jersey **2013**.
[55] M. Soltanzadeh, S. H. Peighambardoust, B. Ghanbarzadeh, S. Amjadi, M. Mohammadi, J. M. Lorenzo, H. Hamishehkar, *Food Hydrocolloids* **2022**, *129*, 107620.
[56] P. Mallick, B. N. Dash, *Nanosci. Nanotechnol.* **2013**, *3*, 130.
[57] AERNOR, UNE-EN ISO 527-3. Plásticos. Determinación de las propiedades en tracción. Parte 3: Condiciones de ensayo para películas y hojas., AENOR. 2019.
[58] S. El, S. Koraichi, H. Latrache, F. Hamadi, *Scanning Electron Microscopy*, InTech, London, UK **2012**.
[59] G. P. Specifications, INTERNATIONAL STANDARD ISO iTeh STANDARD iTeh STANDARD PREVIEW, 2009. https://standards.iteh.ai/catalog/standards/sist/f8d9962b-9afd-4385-bcd0-aa0e0a37a34c/iso-4287-1997-amd-1-2009
[60] T. Li, Y. Wang, X. Wang, C. Cheng, K. Zhang, J. Yang, G. Han, Z. Wang, X. Wang, L. Wang, *Membranes (Basel)* **2022**, *12*, 122.
[61] Y. Qian, C. Wang, F. Gao, *Anal. Chim. Acta* **2014**, *845*, 1.
[62] P. Stafiej, F. Küng, F. E. Kruse, D. W. Schubert, T. A. Fuchsluger, *Biomater. Med. Appl. Res.* **2018**, *2*, 1.
[63] Y. Bu, A. Pandit, *Bioact. Mater.* **2022**, *13*, 105.
[64] P. Wongphan, T. Panrong, N. Harnkarnsujarit, *Food Packag. Shelf Life* **2022**, *32*, 100844.
[65] M. Drobota, S. Vlad, L. M. Gradinaru, A. Bargan, I. Radu, M. Butnaru, C. M. Rîmbu, R. C. Ciobanu, M. Aflori, *Materials (Basel)* **2022**, *15*, 3479.

[66] Y. Mosleh, W. de Zeeuw, M. Nijemeisland, J. C. Bijleveld, P. van Duin, J. A. Poulis, *Adv. Eng. Mater.* **2021**, *23*, 2000716.
[67] K. Chen, J. Yu, J. Huang, Q. Tang, H. Li, Z. Zou. *Int. J. Biol. Macromol*, **2020**, *167*, 1.
[68] H. Zhou, H. Tong, J. Lu, Y. Cheng, F. Qian, Y. Tao, H. Wang, *Carbohydr. Polym.* **2021**, *270*, 118381.
[69] J. W. Rhim, S. I. Hong, H. M. Park, P. K. W. Ng, *J. Agric. Food Chem.* **2006**, *54*, 5814.
[70] M. R. de Moura, F. A. Aouada, R. J. Avena-Bustillos, T. H. McHugh, J. M. Krochta, L. H. C. Mattoso, *J. Food Eng.* **2009**, *92*, 448.
[71] F. M. Vanin, M. H. Hirano, R. A. Carvalho, I. C. F. Moraes, A. M. Q. B. Bittante, P. J. A. do Sobral, *Food Res. Int.* **2014**, *63*, 16.
[72] J. F. Martucci, R. A. Ruseckaite, *Food Hydrocolloids* **2017**, *64*, 70.
[73] I. Benito-González, A. López-Rubio, M. Martínez-Sanz, *Int. J. Biol. Macromol.* **2018**, *118*, 542.
[74] M. Á. V. Rodrigues, M. R. V. Bertolo, C. A. Marangon, V. C. A. da Martins, A. M. G. de Plepis, *Int. J. Biol. Macromol.* **2020**, *160*, 769.
[75] A. S. Spatafora Salazar, P. A. Sáenz Cavazos, H. Mújica Paz, A. Valdez Fragoso, *J. Food Eng.* **2019**, *245*, 73.
[76] M. Junaid, H. Dowlath, S. Anjum, S. B. M. Khalith, S. Varjani, S. Kumar, G. Munuswamy, S. Woong, W. Jin, B. Ravindran, *Environ. Res.* **2021**, *201*, 111585.
[77] M. El Halim, L. Daoudi, A. El Alaoui El Fels, *Color Res. Appl.* **2022**, *47*, 475.
[78] M. Šupová, G. S. Martynková, K. Barabaszová, *Sci. Adv. Mater.* **2011**, *3*, 1.
[79] T. Chatkitanan, N. Harnkarnsujarit, *Meat Sci.* **2021**, *172*, 108367.
[80] A. Radoń, A. Drygała, Ł. Hawełek, D. Łukowiec, *Mater. Charact.* **2017**, *131*, 148.
[81] S. Jalili-Firoozinezhad, M. H. Mohamadzadeh Moghadam, M. H. Ghanian, M. K. Ashtiani, H. Alimadadi, H. Baharvand, I. Martin, A. Scherberich, *RSC Adv.* **2017**, *7*, 39628.
[82] M. Yadav, *Compos. Commun.* **2018**, *10*, 1.
[83] P. Leelaphiwat, C. Pechprankan, P. Siripho, N. Bumbudsanpharoke, N. Harnkarnsujarit, *Food Chem.* **2022**, *369*, 130956.
[84] P. Klinmalai, A. Srisa, Y. Laorenza, W. Katekhong, *LWT* **2021**, *152*, 112356.
[85] L. An, D. Zhang, L. Zhang, G. Feng, *Nanoscale* **2019**, *11*, 9563.
[86] S. Zargarian, V. Haddadi-asl, *Iran. Polym. J.* **2010**, *19*, 457.
[87] S. Abdolmohammadi, S. Siyamak, N. A. Ibrahim, W. M. Z. Wan Yunus, M. Z. Ab Rahman, S. Azizi, A. Fatehi, *Int. J. Mol. Sci.* **2012**, *13*, 4508.
[88] H. B. Hashim, N. A. A. B. Emran, T. Isono, S. Katsuhara, H. Ninoyu, T. Matsushima, T. Yamamoto, R. Borsali, T. Satoh, K. Tajima, *Compos. Part A Appl.Sci. Manuf.* **2022**, *158*, 106978.
[89] J. Villasante, A. Martin-Lujano, M. P. Almajano, *Polymers (Basel)* **2020**, *12*, 1424.
[90] D. Phothisarattana, P. Wongphan, K. Promhuad, J. Promsorn, N. Harnkarnsujarit, *Polymers (Basel)* **2021**, *13*, 4192.
[91] D. Phothisarattana, N. Harnkarnsujarit, *Food Packag. Shelf Life* **2022**, *33*, 100901.
[92] L. Ghasemi-Mobarakeh, M. P. Prabhakaran, M. Morshed, M. H. Nasr-Esfahani, S. Ramakrishna, *Biomaterials* **2008**, *29*, 4532.
[93] J. N. Cabrera, M. M. Ruiz, M. Fascio, N. D'Accorso, R. Minchev, P. Dubois, L. Lizarraga, R. M. Negri, *Polymers (Basel)* **2017**, *9*, 331.
[94] S. Paul, J. P. Saikia, S. K. Samdarshi, B. K. Konwar, *J. Magn. Magn. Mater.* **2009**, *321*, 3621.
[95] J. Wu, S. Chen, S. Ge, J. Miao, J. Li, Q. Zhang, *Food Hydrocolloids* **2013**, *32*, 42.
[96] R. Apak, K. Güçlü, B. Demirata, M. Özyürek, S. E. Çelik, B. Bektaşoğlu, K. I. Berker, D. Özyurt, *Molecules* **2007**, *12*, 1496.
[97] A. H. Mota, N. Duarte, A. T. Serra, A. Ferreira, M. R. Bronze, L. Custódio, M. M. Gaspar, S. Simões, P. Rijo, L. Ascensão, P. Faísca, A. S. Viana, R. Pinto, P. Kumar, A. J. Almeida, C. P. Reis, *Pharmaceutics* **2020**, *12*, 1.

How to cite this article: J. A. A. Abdullah, V. Perez-Puyana, A. Guerrero, A. Romero, *J. Appl. Polym. Sci.* **2023**, *140*(32), e54345. https://doi.org/10.1002/app.54345